Macromolecules

ARTICLE

pubs.acs.org/Macromolecules

Simulation of a Symmetric Binary Mixture of Charged Dendrimers Under Varying Electrostatic Interactions: Static and Dynamic Aspects

K. Karatasos* and I. Tanis

Physical Chemistry Laboratory, Chemical Engineering Department, Aristotle University of Thessaloniki, 54124 Thessaloniki, Greece

Supporting Information

ABSTRACT:

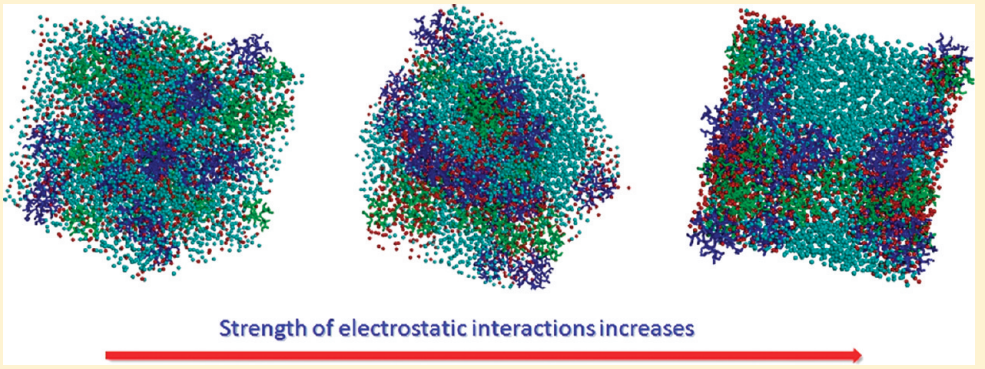

A symmetric binary mixture of terminally charged trifunctional-core/difunctional-branched dendrimers of the third and the fourth generation is examined in explicit solvent solution by means of molecular dynamics simulations. The static and dynamic response of the components is monitored under a varying strength of electrostatic interactions. The response of the dendrimer constituents shares common features as the intensity of Coulombic interactions increases, but characteristic differences are noted in the individual structural arrangement and their dynamic response. An effective-charge modulation develops across the dendritic structure and at the immediate vicinity of each molecule. The asymmetry in size and in the overall charge between the two components affects the packing properties of the molecules resulting in different morphologies compared to the respective single component systems. In addition, individual translational and rotational motion of the dendrimers exhibits distinct behavior in different Coulombic regimes. The motional contrast between the two components differentiates their relative dynamic response as the electrostatic interactions grow stronger. The increase of Coulombic interactions drives the components of the mixture to a dynamically arrested state, but the eventual vitrification takes place at different levels of electrostatic interactions depending on dendrimer generation. The findings of the present study elucidate several aspects of the behavior of these charged soft-colloidal materials and offer new insight toward the control of their long-range order and of their dynamic properties.

I. INTRODUCTION

Control of the structural properties of soft-matter systems in the mesoscale and most recently in the nanoscale dimensions, is the most decisive step toward the design of "smart" functional materials for a broad range of modern applications.[1] In these category of systems, formulations based on mixtures of colloidal particles have attracted an increasing scientific and industrial interest due to the wide range of potential uses, including nanolithography,[2] optoelectronics,[3] sensors,[4] etc. Apart from the common factors that can trigger colloidal aggregation, i.e., concentration, temperature, charge, and external stimuli, colloidal mixtures offer additional control parameters such as the relative size of the colloidal particles and the composition of the mixture, which can be appropriately regulated in order to produce phase diagrams with a rich variety of different morphologies.[5−8]

Although there is already a solid background in the experimental as well as the theoretical description of mixtures of hard-sphere-like particles, systems comprised of soft colloidal particulates of nanosized dimensions have only recently started to be investigated in detail. A characteristic example of such systems are mixtures of multiarm star polymers the behavior of which has lately been examined experimentally,[9−11] theoretically and via computer simulations.[12] An even more recently studied category of soft colloidal materials which can combine the advantages of the polymeric nature (e.g., high rensponsiveness to changes in the local environment) with multifunctionality and with a good control in their size and surface chemistry, are hyperbranched polymers.[13] Because of their unique features, such regularly branched polymers known as dendrimers, have emerged as promising materials for a broad range of uses and, in particular, for applications related to their polyelectrolytic behavior.[14−18] Taking advantage of their intermediate colloid

Received: June 13, 2011
Revised: July 24, 2011
Published: August 01, 2011

and polymeric nature (which endows them with favorable rheological properties) as well as the particularly high concentration of surface active groups in a very small volume, such systems can be very sensitive to changes associated with parameters of the local microenvironment (i.e., pH, ionic strength, external electric field)[19−23] and thus offer the opportunity for a fine control of their structural and dynamic properties.

On the basis of previous theoretical and experimental work in binary charged colloidal mixtures, it is expected that factors such as the relative dimensions of the dendritic components in the mixture, the stoichiometry, the charge distribution and the degree of the screening of the Coulombic interactions, can play a central part in the thermodynamic behavior of a dendrimer mixture as well. In the case of such binary mixtures, relevant theoretical and computational work based on a Gaussian soft potential between uncharged dendrimers, indicated that additional parameters such as the structural details and the dendrimer generation could affect significantly the final equilibrium morphology of these systems.[24]

Although useful insight is provided from the existing studies related to charged colloidal mixtures, or mixtures/blends of uncharged soft-colloidal particles like star polymers and dendrimers, a more detailed investigation of charged dendrimer mixtures is still lacking. Information regarding their self-assembly properties, the specifics of the charge distribution and their response to varying electrostatic interactions could be of particular importance in applications related to their polyelectrolytic behavior. For example, pertinent experiments have demonstrated the advantages of hyperbranched systems over conventional polymeric materials when acting as hosts for ions in solid electrolytes or other electrochemical applications.[14,25] Moreover, their ability to aggregate under the influence of electrostatic interactions[26−32] render them convenient model systems for the examination of self-organization processes in mixtures of charged soft-colloidal particles, much in analogy to their hard-sphere-like analogues.[33,34]

In this context, we have performed a molecular dynamics simulation study of a mixture of terminally charged trifunctional-core/difunctional-branched dendrimers of the third (G3) and the fourth (G4) generation in explicit solvent and counterions. In this work the effects of the variation of the strength of electrostatic interactions are examined in a systematic manner, following the changes imparted in the static and dynamic characteristics of the dendritic components.

II. SYSTEM AND SIMULATION DETAILS

A symmetric mixture of 20 G3 and 20 G4 AB_2 dendrimers was simulated using atomistic (united atom) models for the dendrimers, the solvent beads and the neutralizing counterions, in a wide range of intensities of electrostatic interactions. For the trifunctional core and the bifunctional branching pattern adopted (see Figure S1 in the Supporting Information for a sketch of the dendritic structure), the number of beads per dendrimer molecule as a function of the generation G is given by $N(G) = 1 + 6 \times [2^{G+1} - 1]$. Dendrimers of both generations had the beads of their outer generational shell positively charged (24 in number per G3 molecule and 48 per G4) as in our previous works.[29,30,35] The number of neutralizing counterions amounted to 1440, while that of neutral solvent beads to 4396. The concentration of each dendrimer in the simulation box, C, over the corresponding overlap concentration, C^*, can be estimated via the expression

$$\frac{C}{C^*} = \frac{4\pi N}{3}\left(\frac{R_g}{L}\right)^3 \quad (1)$$

to be 0.03 for G3 and 0.06 for the G4 dendrimers of our system, where R_g and L represent the average radius of gyration and the box size respectively and N the number of dendrimer molecules of each generation, here 20. For comparison purposes, the system was constructed so that the effective concentration C_{eff} if we consider the mixture to be comprised by 40 dendrimers of average size $R_{av}=(R_g^{G3} + R_g^{G4})/2$, is 0.09 C^*_{eff}, i.e., very close to that ($\sim 0.1C^*$) considered in our previous study of one component dendrimer solutions.[29] The adopted forcefield included all the common internal degrees of freedom (i.e, bond stretching, angle bending and torsions) as well as appropriate intra- and intermolecular nonbonded terms, while electrostatic interactions were estimated using full Ewald summation to account for the periodic boundary conditions. The simulations were conducted in the constant volume−constant temperature (NVT) ensemble. The simulation protocol followed and the set of energetic parameters used are the same as those described in ref 29 for the single component systems. All the lengths are given in units of the Lennard-Jones parameter σ between two charged beads, while time is expressed in terms of the characteristic time of our model τ, which corresponds to approximately 1.4×10^3 MD steps. Ensuing to equilibration, trajectories up to $4.5 \times 10^3\tau$ were generated and snapshots were saved with a frequency of 0.7 τ.

Among different equivalent methods of controlling the level of the intensity of the electrostatic interactions in a coarse-grained model (e.g, by changing the ionic strength of the solution, the dielectric permittivity of the solvent or the temperature) we opted in presenting such changes by means of the Bjerrum length (l_B), which relates to the inverse Debye screening length κ^{-1} by

$$\kappa^{-1} = \frac{1}{\sqrt{4\pi l_B \sum_i c_i z_i^2}} \quad (2)$$

In eq 2, c_i and z_i represent the concentration and the valence of ith species of ions in the solution. In our case we consider monovalent ions.

The range of intensities of electrostatic interactions explored, extended from a very weak to a very strong Coulombic regime covering screening lengths in the interval $3 < \kappa R_{av} < 36$ where R_{av} refers to an average radius of gyration of the examined dendrimers. The variation of the screening length in our simulations was performed by appropriate changes in l_B through the relative permittivity ε_r. In experimental conditions a weak electrostatic regime can be realized in polar solvents (e.g., water) and/or in conditions of highly screened electrostatic interactions, while solutions with intermediate or strong Coulombic interactions (with Bjerrum lengths of the order of 10 nm or larger) can be accomplished by appropriate mixtures involving low polarity organic solvents or polar/non polar cosolvent mixtures.[34,36−38] Dendrimer solubilization in organic solvents can be facilitated, e.g., by their appropriate functionalization.[39,40] Alternatively, alteration of the strength of electrostatic interactions can be experimentally realized through changes in temperature and/or the ionic strength of the solution.[41−43] The average size ratio between the two generation dendrimers in our system amounted approximately to $R_g^{G4}/R_g^{G3} \simeq 1.3$, practically independent from

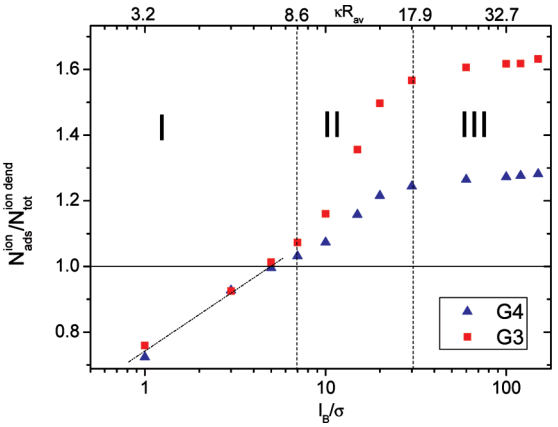

Figure 1. Ratio of the number of condensed counterions over the number of charged beads of the dendrimers of each generation. The horizontal line marks the neutrality limit, while the vertical dotted lines define regimes of distinct behavior of the condensation curves.

the changes in Bjerrum length (see Figure S2 in the Supporting Information).

III. IONIC CORRELATIONS AND STRUCTURAL RESPONSE OF THE DENDRIMERS ON VARIATION OF THE COULOMBIC INTERACTIONS

As has been demonstrated in past computational[6,29,34,42−47] and experimental studies[48−50] in charged soft-colloidal systems and, in particular, in dendrimer solutions,[44,51] the nature of the effective interactions between the solutes are strongly affected by the presence of counterions. Effects like the counterion-mediated attraction of like-charged macroions play a crucial role in their final arrangement and ultimately in the phase behavior of such systems.[8,51−53] Even in the presence of monovalent counterions, experimental[50] and computer simulation studies[29,42,46] indicated that counterion correlation effects affect appreciably the static and dynamic properties of the macroions and are closely associated with deviations from the Poisson−Boltzmann theory.[6,47] Such deviations have already been described theoretically[54] and were found to be consistent with the behavior observed in dendrimer polyelectrolytes.[29] In cases where strong Coulombic interactions are present, the counterion-induced attraction between the dendrimers combined with ionic-correlation effects may lead to the overcharging of the dendritic molecules.[29,42,43] These effects along with specific aspects of the structural changes of the dendrimers upon variation of the level of electrostatic interactions, are described in detail in the next paragraphs.

1. Counterion Condensation and Charge Distribution. To check the degree of counterion condensation on the dendritic molecules of the two different generations upon variation of the intensity of electrostatic interactions, we have estimated the number of "pairs" consisting of a dendrimer charged bead and a counterion. A "pair" is only counted if the distance between a dendrimer's charged bead and a counterion is closer than the first minimum of the corresponding pair correlation function (see Figure S3 in the Supporting Information) and each counterion is taken to participate in one such pair. To better understand the effects of dendrimer size and surface charge density on the degree of counterion condensation, we have calculated the average number of the aforementioned pairs separately for each dendrimer generation. Figure 1 depicts the "condensation curves" for each generation, describing the number of condensed counterions normalized to the number of charged dendrimer beads.

By visually inspecting the dependence of the degree of counterion condensation as a function of Bjerrum length, we can recognize 3 distinct regimes. Regime **I**, corresponding to a domain of weak electrostatic interactions in which the degree of counterion condensation is practically independent from the dendrimer generation, regime **II**, demarcated by the overstepping of the neutrality limit and described by a significant increase of the ratio but at a different rate with respect to l_B among the two dendrimer generations, and regime **III** of strong electrostatic interactions characterized by a gradual leveling-off of the condensation curves. As has been argued in the case of single dendrimer solutions,[29] this overcharging state can be attributed to a population of counterions which are "shared" between neighboring dendrimer molecules. On the basis of the plateau values of the ratios for dendrimer molecules of the two generations, we can actually estimate the number of these "shared" counterions. Indeed, an overcharging percentage of about 30% for the G4 dendrimers, corresponds to a number of $0.3 \times 20 \times 48 = 288$ additional counterions in the vicinity of the G4 charged beads, which can account, to a good approximation, for the degree of overcharging observed in the G3 dendrimers as well, i.e., $288/(20 \times 24) = 0.6$. In other words, almost 20% of the total number of neutralizing counterions are shared between the dendrimers of the two generations in the strong Coulombic regime.

Apart from the actual number of charges associated with the molecules, in soft polyeletcrolye systems with internal degrees of freedom (such as dendrimers, DNA, proteins etc.) the effective charge distribution is also found to be important.[50,52,53]

To obtain a better overview of the effective charge throughout the dendritic structure as well as at the surrounding area around a dendrimer molecule, we have constructed the overall charge distributions with respect to the center of mass of the dendrimes, taking into account the charges of each dendrimer, those of the neighboring dendrimer molecules (irrespective of generation) and the counterions. The resulting profiles are presented in Figure 2.

The most prominent features are the pattern of the charge modulation throughout the dendritic structure and the systematic development of a negative-charge minimum and a positive-charge peak in the immediate vicinity of each dendrimer's periphery, as the strength of electrostatic interactions increases. In the smaller size dendrimers, a shallow negative-charge minimum can also be observed at distances just below the radius of gyration of the dendrimer. This can be understood as a combined effect of the diminishing degree of backfolding (and thus of a lower probability for the terminal positive charges to be detected deeply within the dendritic structure) as Bjerrum length increases, and the higher structural flexibility of the G3 compared to the G4 dendrimers, which facilitates a larger percentage of counterions to penetrate in their interior. The drop in amplitude of the positive peak extending between the radius of gyration and the border of the dendrimer's periphery as l_B increases, can be considered as a direct consequence of the overcharging effect discussed earlier, due to the attraction of a larger number of counterions which become increasingly localized close to the dendrimers' termini. The same argument can also rationalize the negative-charge minimum which deepens as the electrostatic interactions grow stronger, indicating again an increasing population of counterions that become localized close to dendrimer's

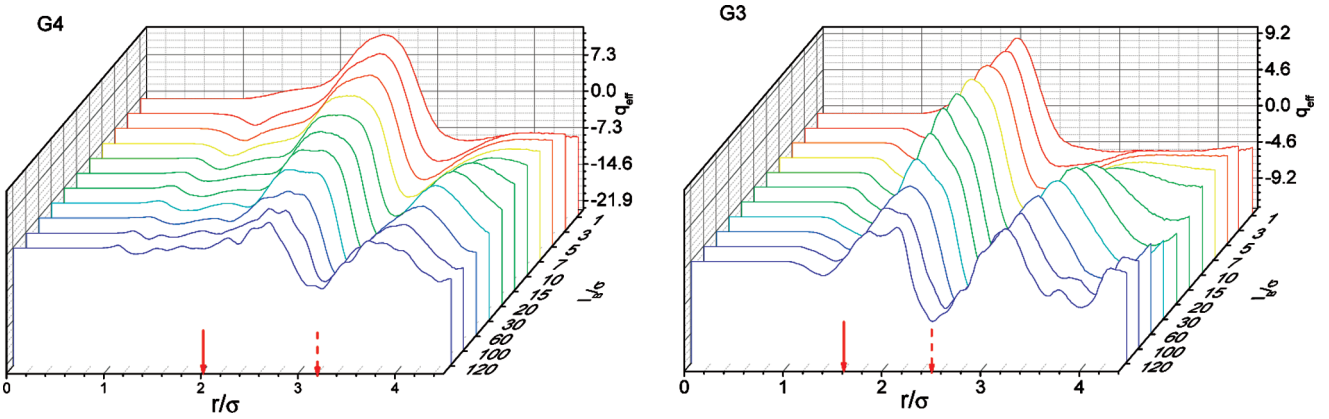

Figure 2. Effective charge distributions for the G3 and G4 dendrimers with respect to the center of mass of the dendrimers as a function of Bjerrum length. The solid arrows denote the location of the radius of gyration of each dendrimer while the dashed arrows mark the maximum distance from the center of mass, at which dendrimer beads can be detected.

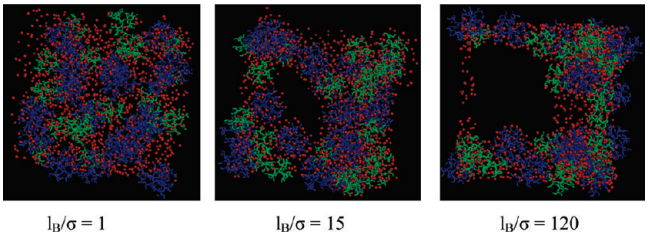

Figure 3. Snapshots of the binary dendrimer mixture at three values of Bjerrum length representing the different electrostatic regimes discussed in the text. Blue and green colors correspond to the G4 and G3 dendrimers respectively, while red dots correspond to the counterions. Solvent beads are omitted for clarity.

periphery. These counterions seem to be "trapped" in-between the two positive-charge peaks, lending credence to the picture of a population "shared" between the neighboring dendrimers, as discussed earlier.

The buildup of the positive-charge peak beyond the dendimer's boundary can be ascribed to the approaching of the neighboring dendrimers due to the counterion-induced like-charge attraction as discussed in the one component systems[29] (see Figure S4 in the Supporting Information for an estimation of the effective potential between dendrimers in the binary mixture). A visual impression of both, the counterion condensation and the dendrimers' approach as the intensity of Coulombic interactions increases, is provided in Figure 3, where snapshots of the simulation box are shown in the three electrostatic regimes of Figure 1.

Starting from regime II (here represented by $l_B/\sigma = 15$) and moving toward regime III (here represented by $l_B/\sigma = 120$), the denser packing of the dendrimer molecules and the localization of the counterions close to the dendrimers becomes evident.

2. Spatial Correlations and Dendrimer Ordering. On the basis of the picture described in the preceding paragraph and according to findings in the single generation dendrimer solutions,[29,30] increase of the strength of electrostatic interactions triggers the onset of strong spatial correlations between the ionic species (i.e, counterions and charged dendrimer beads). In the examined case of the binary mixture it is of interest to examine whether the existence of size mismatch and surface charge density contrast (G4 dendrimers possess 25% higher surface charge density compared to G3 molecules) between the two different dendrimer generations, can give rise to distinct responses concerning such spatial correlations upon Bjerrum length variation.

Figure 4 shows the spatial correlation functions between pairs of charged beads belonging to distinct dendrimer molecules of the same (Figure 4a and Figure 4b) and of different (Figure 4c) generations.

The pair correlation functions describing the two dendrimer generations share common features, such as the shift of the main peak to shorter distances as the strength of electrostatic interactions increases, as well as the appearance of additional sharp peaks at shorter distances in l_B values within regime **III**, denoting a close proximity and a local ordering of the charged beads forming the examined pairs. A distinct feature, however, which differentiates the response of the two different dendrimer generations, is an abrupt change observed in the correlation functions of the G3 molecules, upon changing of Bjerrum length from 10σ to 15σ, which is absent from the corresponding G4 spectra. The same correlation functions describing the G3−G4 charged-bead pairs exhibit a degree of change which is intermediate between the abrupt and the moderate change observed in the G3 and the G4 spectra respectively, in the transition from $l_B = 10\sigma$ to $l_B = 15\sigma$ values. Such a sensitive response of local spatial rearrangements of the charged beads in G3 dendrimers, is consistent with the higher degree of structural deformability of the G3 molecules compared to the more compact and thus less deformable structure of the G4 dendrimers,[55] which increases the probability of counterion penetration within the structure of the former.

This difference between the ability of G3 and G4 dendrimers to deform, their difference in size and their distinct surface charge densities are expected to influence also the spatial arrangement in length scales comparable to their size or even longer. To follow such long-length scale responses to the variation of the strength of electrostatic interactions, we have calculated the static structure factor arising from the centers of mass of the dendrimers invoking eq 3

$$S_{cm}(q) = \left\langle \left\langle \frac{1}{N} \left| \sum_{i=1}^{N} e^{i\,\vec{q}\cdot\vec{r}_i} \right|^2 \right\rangle_{|q|} \right\rangle_{directions} \quad (3)$$

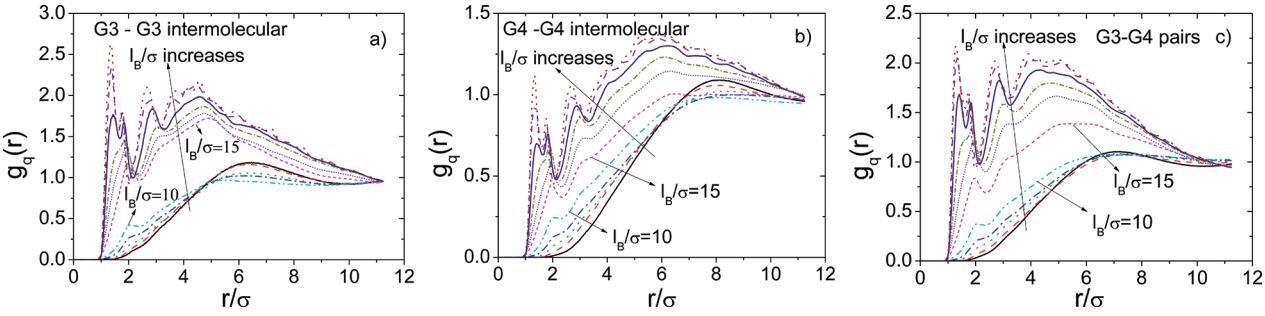

Figure 4. Intermolecular pair correlation functions between the charged terminal beads, for (a) G3−G3 pairs, (b) G4−G4 pairs, and (c) G3−G4 pairs. Long arrows point to the direction of increase of Bjerrum length, while short arrows specify the $l_B/\sigma = 10$ and $l_B/\sigma = 15$ values as discussed in the text.

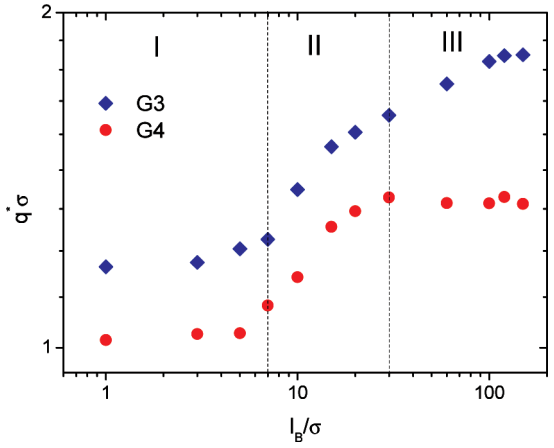

Figure 5. Dependence of the q-value of the examined structural peak of the static structure factor arising from the centers of mass of the dendrimers, on Bjerrum length. The vertical lines denote the boundaries of the different electrostatic regimes as defined in Figure 1.

To avoid any assumptions regarding the isotropy of the system at different Bjerrum lengths, we have calculated the structure factor by averaging over 50 directions uniformly distributed on the surface of a sphere for each magnitude of the scattering vector $|q|$ (henceforth denoted as q).[29] In eq 3, N represents the number of scatterers which, in our case, is the number of dendrimer molecules. This calculation was performed separately for the centers of mass of the G3 and G4 molecules, in order to monitor possible effects arising from the difference in generation. To map the packing characteristics of the dendrimer molecules as Bjerrum length increases, we have monitored the shift of the structural peak which corresponds to a length scale comparable to the dimensions of the dendrimers (i.e., of the order of $2R_g$), in analogy to the procedure followed in the single component dendrimer solutions.[29] Figure 5 depicts the dependence of the q-value corresponding to the maximum of that structural peak (denoted as q^*) as a function of l_B.

Evidently, the boundaries defined earlier based on the counterion condensation dependence on Bjerrum length, appear to provide a sound definition of the l_B domains in which the packing of the dendrimers exhibits distinct patterns, as well.

This is a clear indication for a direct link between the degree of counterion condensation and the adopted dendrimer arrangement in the mixture, in line with the observations made in the one component solutions.[30] The stronger dependence of the spatial arrangement of both generation dendrimers on l_B takes place in the intermediate electrostatic regime, while a plateau-like behavior characterizes the very weak and very strong electrostatic regimes. The leveling-off of the G3 dendrimers' dependence in regime III appears to be attained only at the higher l_B values examined. This might be associated with the significantly higher degree of overcharging realized at the G3 systems (Figure 1), but it could also relate to the different degree of dynamic slow-down experienced by the two different dendrimer generations as will be discussed in section IV.

In one component dendrimer polyelectrolyte solutions, the result of the spatial rearrangement of the dendrimer molecules in the strong electrostatic regime at similar overall concentration, was the formation of distinct cubic phases with a symmetry depending on the dendrimer generation.[29−31] In these cases the molecular packing was not affected by size polydispersity that could trigger structural frustration.[7] Experimental investigations in bidisperse like-charged colloidal suspensions[56] demonstrated that the observed morphologies also differed compared to those characterizing the pure components and remained as an open question whether the mixed-crystal structures found, could actually be a form of a superlattice. On these accounts, parameters like the average size ratio between the molecules in the examined system (R_g^{G4}:R_g^{G3} ≃ 1:1.3), the structural flexibility of the dendrimers and the observed charge distribution (Figure 2), are likely to differentiate the packing characteristics at the molecular scale (particularly in the strong Coulombic regime), with respect to those observed in the single component solutions.[7,30]

The static structure factor spectra (eq 2) corresponding to the strong electrostatic regime ($l_B/\sigma = 120$) are shown separately for the G3 and the G4 molecules in Figure 6.

The same structural features appearing in Figure 6, characterize also the respective spectra for the other l_B values residing within the strong electrostatic regime (see Figure S6 in the Supporting Information). A visual inspection of the resulted spectra shows that structural ordering of the two dendrimer constituents does take place in the binary mixture, as well. The lower-q maximum close to $q\sigma \cong 0.5$ which is present in spectra of both dendrimer generations, remains practically l_B-independent in location (for the full set of spectra see Figure S5 in the Supporting Information), once the strength of the Coulombic interactions grows larger than the values in the weak electrostatic range. This low-q peak which was also present in the single component systems,[29] is indicative for the existence of long-length scale structural inhomogeneities (e.g., ordered structures) and has been detected experimentally in other hard or soft-colloidal systems as well.[50,57] For the examined system, such large-scale inhomogeneities can be recognized already from the snapshots in

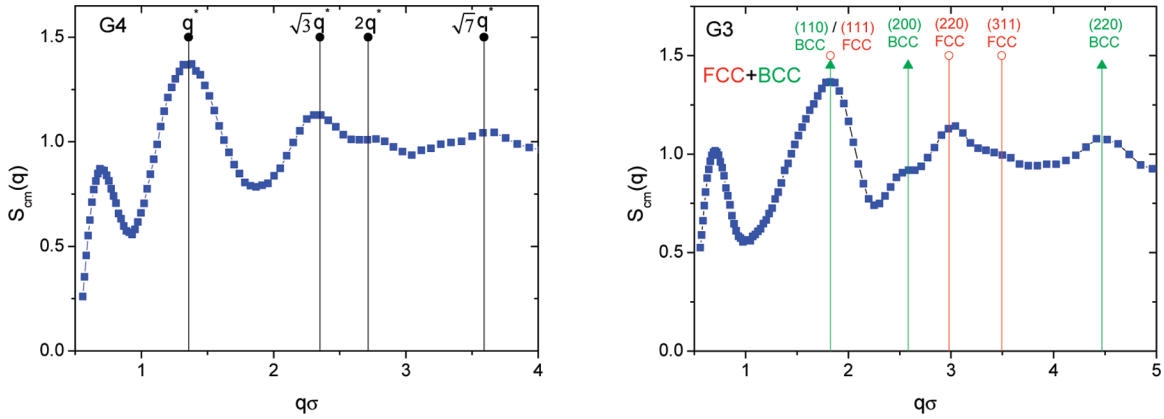

Figure 6. Static structure factor arising from the centers of mass of the dendrimer molecules for G4 (left) and G3 (right) dendrimers, at $l_B/\sigma = 120$. Vertical lines denote characteristic peak locations aiming at the identification of the structure. For G3 molecules, Miller indices corresponding to characteristic lattice planes of FCC and BCC crystals are shown as well.

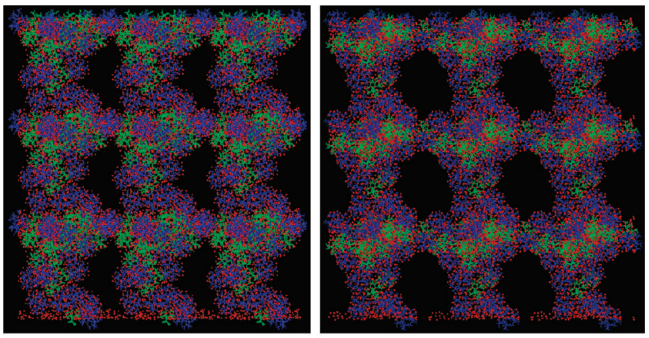

Figure 7. Snapshots shown in Figure 3 for $l_B/\sigma = 15$ and $l_B/\sigma = 20$, together with periodic images of the simulation box (solvent beads are omitted for clarity).

Figure 3 . For better visual identification, in Figure 7 we redraw the snapshots of the system in $l_B/\sigma = 15$ and $l_B/\sigma = 120$ of Figure 3 together with periodic neighbors of the simulation box.

Long-range inhomogeneities emerging from spatial correlations between dendrimer molecules separated from the solvent-filled space (here depicted as void), are compatible to the presence of the lower-q peak of the static structure factor (Figure 6).

Focusing now on the structural features as described by the higher-q peaks, it appears that the spatial arrangement of dendrimers of the two different generations exhibit different characteristics. For the larger generation G4 dendrimers, the scattering spectra are consistent with a random close-packed-like local structure. X-ray scattering spectra indicating similar spatial arrangement have been experimentally detected in high concentration charged colloid suspensions.[8] Those systems exhibited a glass-like phase much in analogy to that observed in metallic glasses[58] and supercooled amorphous bidisperse Lennard-Jones liquids.[59] The similarity in structure between the G4 dendrimers and that observed in the colloidal systems, implies that at the strong Coulombic regime the G4 dendrimers of the binary mixture become "arrested" in a structurally frustrated state, in contrast to their behavior in the single component system where an FCC crystal phase was formed[29] under the same strength of electrostatic interactions. A discrepancy between the adopted structure in the binary mixture and that in the corresponding one component system is observed for the G3 dendrimers as well. While in the single G3 solution dendrimers were organized in a BCC phase,[29] in the binary dendrimer mixture it appears that the G3 molecules form a BCC/FCC mixed domain at the same electrostatic regime (Figure 6). Similar mixed lattice phases have previously been observed in other charged colloidal systems, such as in peripherally charged star polymers[49] and in binary mixtures of like-charged colloidal spheres.[5] In those cases the parameters which determined the phase behavior of the studied systems were either concentration/number density or composition.

On the basis of the previous knowledge of the single component systems[29,30,35] and the indications discussed above, it appears plausible to consider the dynamic contrast between the G3 and G4 molecules[55,60] as a possible factor which intervenes in the ordering process, affecting thus the (pseudo)-equilibrium final morphology of the system. This picture is also consistent with the fact that in regime III (Figure 5), the plateau of q^* for G4 dendrimers is reached at a lower l_B value compared to that of the G3 molecules, implying that the rearrangement of the G3 molecules continues to take place in a practically "fixed" local environment formed by the G4 molecules.

IV. DYNAMIC RESPONSE OF THE DENDRIMERS

To further elaborate on the dynamic behavior the dendrimers of the two generations, we have examined aspects of the translational and rotational motion of the molecules upon variation of the intensity of electrostatic interactions. The dynamic probes invoked are related to experimentally observable quantities and therefore offer the possibility for comparison whenever results of such experiments become available for similar systems.

1. Dynamics of Structural Rearrangements in the Dendrimer Scale. Individual motion of the G3 and the G4 dendrimers was examined via the incoherent dynamic structure factor arising from the centers of mass of molecules, according to eq 4, which is the time dependent version of eq 3.

$$S_{cm}^{inc}(q,t) = \left\langle \frac{1}{N} \langle \sum_{i=1}^{N} e^{-i\,\vec{q}\cdot[\vec{r}_i(t) - \vec{r}_i(0)]} \rangle_{|q|} \right\rangle_{directions} \quad (4)$$

The symbols appearing in eq 4 are as in eq 3. This function probes density fluctuations of the scatterers at different time and length scales. It can be obtained through experiments which can

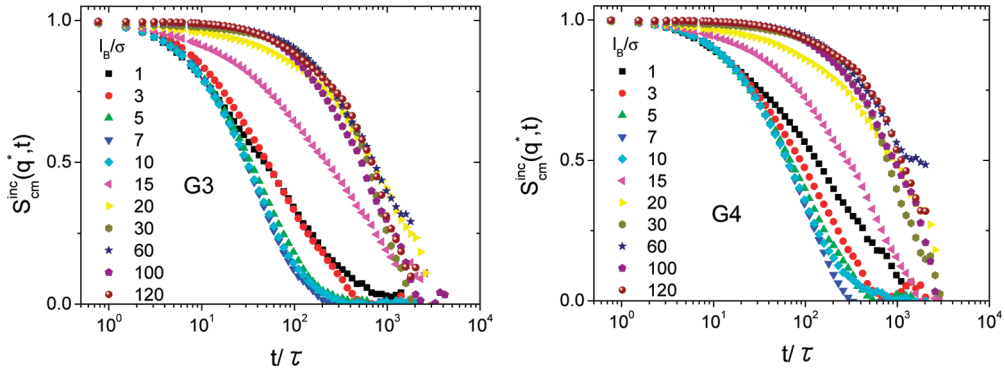

Figure 8. Incoherent dynamic structure factor data for the G3 (left) and the G4 (right) dendrimers, at $q = q^*$, for all the examined Bjerrum lengths.

provide both, spatial and temporal resolution, such as neutron scattering. To examine dynamics of structural rearrangements in the dendrimer scale, we have calculated $S_{cm}^{inc}(q,t)$ at a q-magnitude equal to q^*. Figure 8 shows the scattering spectra obtained, separately for the G3 and the G4 molecules.

Evidently, there is a strong dependence of the dynamic response in the molecular scale on the variation of the intensity of electrostatic interactions. The most drastic changes appear to take place when passing from the weak, (i.e., $l_B/\sigma \leq 7$) to the intermediate (i.e., $7 \leq l_B/\sigma \leq 30$) electrostatic regime. To quantify the observed behavior, we have estimated the average relaxation time by calculating the area under the corresponding curve according to eq 5

$$\langle t \rangle_{cm} = \int S_{cm}^{inq}(q^*, t)\, dt \qquad (5)$$

To avoid possible underestimation or overestimation of the average time, we performed the integration only to those curves which have relaxed almost entirely (i.e., more than 90%) within the simulation window. The result of this calculation is presented in Figure 9. Following the dynamic response of the centers of mass of the dendrimers in a length scale comparable to their size, it becomes clear that the latter is strongly correlated to the respective static changes which take place when varying the intensity of Coulombic interactions (Figure, 5).

In regime **I**, a moderate speed-up of the individual dendrimer motion can be observed, followed by a noticeable slow-down when the strength of electrostatic interactions increases within regime **II**. This slow-down appears to cease in regime **III**, where a virtual "freezing-in" of the dendrimer motion takes place upon further increase of l_B.

It is worth noticing that practically at all cases, the average relaxation time of the G3 dendrimers is lower compared to that of G4, even in regime **III**, as would be anticipated due to their smaller size and higher structural flexibility which facilitates their diffusional motion.

The aforementioned dynamic pattern can be interpreted in conjunction with the behavior described earlier regarding the counterion condensation process (Figure 1) and the modulation of the effective charge in the dendrimer's vicinity (Figure 2). While the dendrimers lie in the weak electrostatic regime and below the "neutrality" limit (see Figure 1), increase of the electrostatic interactions result to stronger repulsions between the like-charged molecules which may incur faster rearrangements. As the neutrality limit is reached (i.e., in the transition from regime I to regime II), further increase in the intensity of the

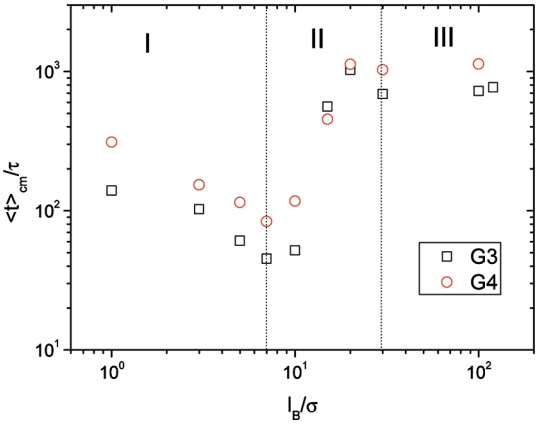

Figure 9. Average relaxation times corresponding to spectra appearing in Figure 8. The dashed lines mark the boundaries between the different electrostatic regimes, denoted as **I**, **II**, and **III**.

electrostatic interactions results in the overcharging of the dendrimers and thus to like-charge attraction. This effective attraction brings the dendrimers at much closer distances (see Figure 5) creating thus a local "jamming". Such a close packing of the molecules is consistent with the slowing-down observed in regime **II**. In regime **III**, no significant changes in the counterion condensation process and the effective charge seem to occur upon increase of l_B (Figure 1 and 2), while the average distance between molecules (see Figure 5) appears either to remain unchanged (in G4) or to reach a limiting value at the higher l_B levels (G3). This scenario implies a virtually "frozen" state of the local environment experienced by the dendrimer molecules which renders $\langle t \rangle_{cm}$ insensitive to a further increase of l_B.

To elaborate more on the specifics of this progressive "vitrification" of the local environment as l_B increases, we have monitored the variation of the dimensions of the "cage" formed by the immediate neighbors of each dendrimer molecule as the strength of electrostatic interaction increases. An estimation of this cage size can be obtained by the location of the inflection point of the mean squared displacement of the centers of mass of the molecules, in the transition from the ballistic motion at short times to the restricted diffusion at longer time scales (prior to the free diffusion regime); in this time- and length scale, the presence of the neighboring molecules start to obstruct the translational motion of the particles (here the dendrimer molecules).[11,60]

Figure 10 illustrates the changes of the cage dimensions as the system goes through the intermediate and the strong electrostatic

dx.doi.org/10.1021/ma2013282 |*Macromolecules* 2011, 44, 6605–6614

regimes (in regime **I**, no inflection point is present). Apparently, the size of the cage scales with l_B in both electrostatic domains, with the dependence becoming weaker when passing from the intermediate to the strong Coulombic regime. The inset of Figure 10 depicts the ratio of the cage size over the intermolecular dendrimer distance which corresponds to the main structural peak (q^*) of the respective static structure factor. This ratio provides a direct probe for the examination of the validity of the Lindemman criterion for melting (or freezing-in)[61] which is known to apply in a wide range of glass-forming systems.[8,11,62]

As the intensity of electrostatic interactions increases, the ratio describing the G4 dendrimers approaches a value close to 0.1 which is consistent with the aforementioned Lindemann's criterion, indicating that the larger size dendrimers behave similarly to conventional glass-forming particles when approaching a freezing-in transition. The same ratio also decreases upon increase of l_B for the G3 molecules but remains systematically higher compared to that of the G4 dendrimers. This notion corroborates our earlier argument that the G3 molecules retain a higher degree of mobility compared to the larger size molecules even in the strong electrostatic regime and lies in agreement with the faster $\langle t \rangle_{cm}$ times observed for the G3 dendrimers (Figure 9).

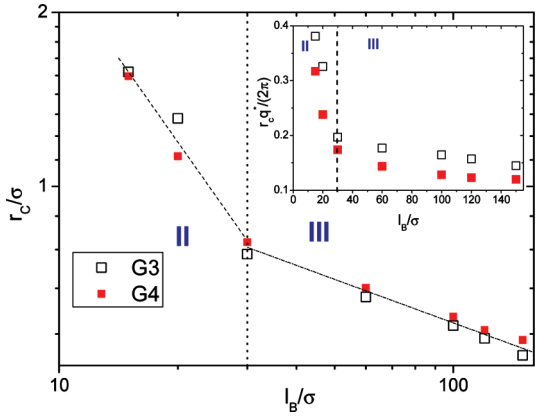

Figure 10. Dependence of the cage size experienced by the dendrimers of the two generations (main panel). The vertical dotted line marks the boundary between regime **II** and regime **III** of electrostatic interactions, while the dashed straight lines show indicative scalings of the cage size with l_B (slope = −1 and −0.25 for regime **II** and regime **III**, respectively). Inset shows the corresponding ratio of the cage size over the length scale ($2\pi/q^*$) corresponding to the main structural peak of the static structure factor.

2. Reorientational Dynamics of the Dendrimers. An additional dynamic process which contributes to the local rearrangement of dendimers, is the overall rotational motion of the molecules. For dendrimers, an appropriate dynamic probe is, for instance, the calculation of the second order Legendre polynomial

$$G_2(t) = \frac{1}{2}\langle 3[\hat{\mathbf{h}}(t)\cdot\hat{\mathbf{h}}(0)]^2 - 1\rangle \quad (6)$$

where $\hat{\mathbf{h}}$ represents unit vectors which connect the center of mass of each molecule with the beads belonging to the outer generational shell of the dendrimer. Such a correlation function essentially relaxes via the reorientational motion of the entire molecule,[42,63,64] and can be accessed experimentally with spectroscopic techniques such as neutron magnetic resonance measurements[64,65] and dielectric relaxation spectroscopy[66] (the latter technique requires the existence of a permanent dipole moment and probes the first order Legendre polynomial, but the essence of the information obtained remains the same).

The reorientational spectra calculated separately for the two different generations in the examined electrostatic regimes are presented in Figure 11. As in the case of the individual translational motion of the dendrimers (Figure 8), increase of the strength of electrostatic interactions slows-down the overall rotational motion of the dendrimers.

Actually, the retardation in the reorientational motion of the molecules is drastic even in the intermediate electrostatic regime ($7 \le l_B/\sigma \le 30$) leading to a virtual freezing-in of the molecular rotation upon further increase of l_B (regime III). Following a similar procedure as before (section IV.1), an average rotational relaxation time was calculated by integrating the corresponding $G_2(t)$ functions appearing in Figure 11 (the procedure was applied only to spectra with a degree of decorrelation not lower than 90%). Figure 12 depicts the obtained average times as a function of Bjerrum length. Because of the low decorrelation degree of the respective $G_2(t)$ spectra, only values in the weak (**I**) and the intermediate (**II**) electrostatic regimes could be obtained.

As in the previous static and dynamic properties discussed earlier, the behavior of the rotational relaxation time shows distinctly different characteristics in the two electrostatic regimes. In both regimes dendrimer rotational times are proportional to the intensity of electrostatic interactions, however, in regime **I** only a weak increase is observed with l_B, while in regime **II** dendrimer rotation undergoes a drastic slow-down. The smaller size dendrimers reorient faster as anticipated,[63,64] while it should

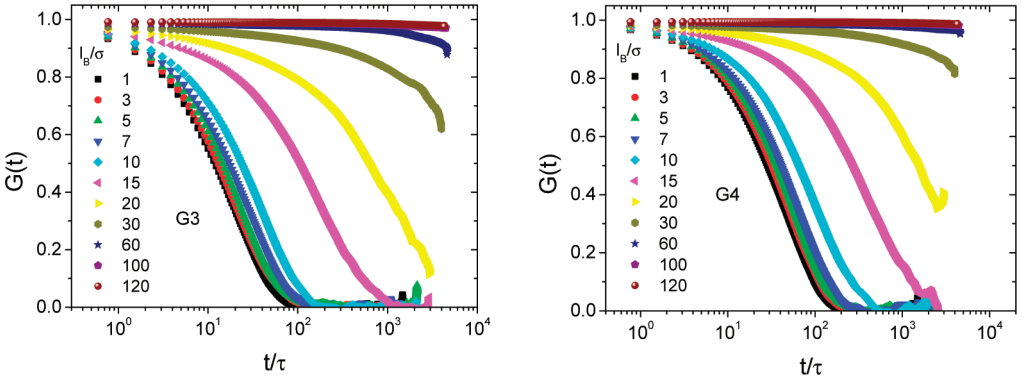

Figure 11. Rotational relaxation spectra (eq 5), for the G3 (left) and the G4 (right) dendrimers.

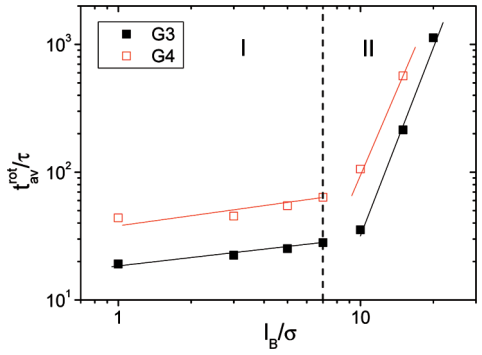

Figure 12. Average dendrimer reorientational times as a function of Bjerrum length. The straight lines are guides to the eye. The vertical dashed line marks the boundary between the weak (**I**) and the intermediate (**II**) electrostatic regime.

also be noted that the time scale of the rotational motion for both dendrimer generations is of the same order of magnitude with that for the individual translational motion (Figure 9). This similarity in time scale implies a coupling between the two distinct dynamic modes.

V. SUMMARY/CONCLUSIONS

In this work we have examined a symmetric, in terms of composition, binary dendrimer mixture, with explicit counterions and solvent molecules and retaining the internal degrees of freedom of the dendritic structure. The static and dynamic features of the individual components were examined in a wide range of Bjerrum length values, covering a weak, an intermediate and a strong electrostatic regime. The response of the morphological characteristics of the mixture as described by the spatial arrangement of the dendrimers, as well as that of the dynamic behavior of the components in the length scale of the molecular size, was found to be rather sensitive and thus potentially detectable by future relevant experiments.

The distinct features of the two polymeric constituents, such as the difference in the average size, in the degree of structural flexibility and in the total charge per dendrimer, affected the level of their response to the variation of the strength of Coulombic interactions. Because of the exactly half number of charged beads per molecule, G3 dendrimers experienced twice as high a degree of overcharging compared to the G4 molecules. This effect was triggered by an increasing degree of spatial correlations between the charged beads and the counterions as the intensity of electrostatic interactions grew stronger. A characteristic effective-charge pattern was formed across the dendritic structure and the immediate vicinity, stemming by a population of "shared" counterions (about 20% of the total) in the region of interpenetration between the neighboring molecules (this effect of counterion localization might be of particular importance in applications related to ion storage).

The spatial arrangement in a length scale comparable to the size of the dendrimers, appeared to be strongly affected by the variation of the strength of Coulombic interactions, particularly in the intermediate regime (II) within which the degree of dendrimer overcharging increased the most.

By monitoring the behavior of the two different generations in the mixture, it was found that the relative spatial arrangement of the G3 and G4 dendrimers, differentiated markedly with respect to the morphologies observed in the corresponding one component mixtures.[29] Instead of FCC (G4) and BCC (G3) cubic phases that were formed in the latter under similar conditions, random-closed-packed-like (G4) and mixed BCC/FCC (G3) structures were found to describe better the packing of the components in the binary system.

These observations regarding the packing characteristics of the dendrimers in the mixture, indicated that the "frustrated" local structures could be linked to the distinct dynamic features of the two generations. The individual translational and rotational motion of the larger size dendrimers was realized at longer time scales in all electrostatic regimes. This motional contrast between dendrimers of the two generations was reflected to the dynamic characteristics of the surrounding microenvironment, leading to a virtual "freezing-in" of the G4 molecules at comparatively lower levels of electrostatic interactions. The observed structural characteristics of the local environment in the mixture, in conjunction with the presence of dynamic signatures associated with a motional arrest which is commonly met in soft and hard-colloidal glassy systems,[9,11,55,62,63,67,68] indicated that dendrimer electrolytes (particularly those of high generation) can essentially be viewed, under the examined conditions, as soft-colloidal glass forming materials. In this case, electrostatic interactions can be considered to act as a pseudo-thermodynamic inverse temperature,[37] offering the possibility to control the ordering characteristics of such systems.

■ ASSOCIATED CONTENT

Ⓢ Supporting Information. Schematic of the dendritic structure of the models adopted in the current work, variation of the average radius of gyration for the two dendrimer components of the binary mixture, pair correlation functions between counterions and charged dendrimer beads, effective interaction potential between the dendrimer molecules, and static structure factors. This material is available free of charge via the Internet at http://pubs.acs.org.

■ AUTHOR INFORMATION

Corresponding Author
*E-mail: karatas@eng.auth.gr.

■ ACKNOWLEDGMENT

The present study was performed in the framework of the ESF COST action TD0802.

■ REFERENCES

(1) Löwen, H. *J. Phys.: Condens. Matter* **2001**, *13*, R415–R432.
(2) Mikrajuddin; Iskandar, F.; Okuyama, K. *Adv. Mater.* **2002**, *14* (12), 930–933.
(3) Galisteo-Lopez, J. F.; Ibisate, M.; Sapienza, R.; Froufe-Perez, L. S.; Blanco, A.; Lopez, C. *Adv. Mater.* **2011**, *23* (1), 30–69.
(4) Hagleitner, C.; Hierlemann, A.; Lange, D.; Kummer, A.; Kerness, N.; Brand, O.; Baltes, H. *Nature* **2001**, No. 414, 293–6.
(5) Lorenz, N. J.; Palberg, T. *J. Chem. Phys.* **2010**, *133* (10), No. 104501.
(6) Dijkstra, M. *Curr. Opin. Colloid Interface Sci.* **2001**, *6* (4), 372–382.
(7) D'Aguanno, B.; Méndez-Alcaraz, J.; Klein, R. Structure and thermodynamics of mixtures of charged spherical colloidal particles. In

Trends in Colloid and Interface Science V, Corti, M., Mallamace, F., Eds.; Springer: Berlin and Heidelberg, Germany, 1991; Vol. 84, pp 381−390.
(8) Sirota, E. B.; Ou-Yang, H. D.; Sinha, S. K.; Chaikin, P. M.; Axe, J. D.; Fujii, Y. *Phys. Rev. Lett.* **1989**, *62* (13), 1524.
(9) Mayer, C.; Sciortino, F.; Likos, C. N.; Tartaglia, P.; Löwen, H.; Zaccarelli, E. *Macromolecules* **2009**, *42* (1), 423–434.
(10) Mayer, C.; Stiakakis, E.; Zaccarelli, E.; Likos, C.; Sciortino, F.; Tartaglia, P.; Löwen, H.; Vlassopoulos, D. *Rheol. Acta* **2007**, *46* (5), 611–619.
(11) Mayer, C.; Zaccarelli, E.; Stiakakis, E.; Likos, C. N.; Sciortino, F.; Munam, A.; Gauthier, M.; Hadjichristidis, N.; Iatrou, H.; Tartaglia, P.; Lowen, H.; Vlassopoulos, D. *Nat. Mater.* **2008**, *7* (10), 780–784.
(12) Hoffmann, N.; Likos, C. N.; Lowen, H. *J. Chem. Phys.* **2004**, *121*, 7009.
(13) Jikei, M.; Kakimoto, M. *Prog. Polym. Sci.* **2001**, *26* (8), 1233–1285.
(14) Astruc, D.; Boisselier, E.; Ornelas, C. *Chem. Rev.* **2010**, *110* (4), 1857–1959.
(15) Li, X.; Zamponi, M.; Hong, K.; Porcar, L.; Shew, C. Y.; Jenkins, T.; Liu, E.; Smith, G. S.; Herwig, K. W.; Liu, Y.; Chen, W. R. *Soft Matter* **2011**, *7* (2), 618–622.
(16) Tanis, I.; Karatasos, K. *Phys. Chem. Chem. Phys.* **2009**, *11*, 10017–10028.
(17) Chen, C. M.; Fang, X. L. *J. Appl. Polym. Sci.* **2010**, *117* (6), 3539–3544.
(18) Storkle, D.; Duschner, S.; Heimann, N.; Maskos, M.; Schmidt, M. *Macromolecules* **2007**, *40* (22), 7998–8006.
(19) Chen, W.; Tomalia, D. A.; Thomas, J. L. *Macromolecules* **2000**, *33*, 9169–9172.
(20) Ramzi, A.; Scherrenberg, R.; Joosten, J.; Lemstra, P.; Mortensen, K. *Macromolecules* **2002**, *35* (3), 827–833.
(21) Criscione, J. M.; Le, B. L.; Stern, E.; Brennan, M.; Rahner, C.; Papademetris, X.; Fahmy, T. M. *Biomaterials* **2009**, *30* (23−24), 3946–3955.
(22) Guillot-Nieckowski, M.; Joester, D.; Stöhr, M.; Losson, M.; Adrian, M.; Wagner, B.; Kansy, M.; Heinzelmann, H.; Pugin, R.; Diederich, F.; Gallani, J.-L. *Langmuir* **2006**, *23* (2), 737–746.
(23) Giupponi, G.; Buzza, D. M. A.; Adolf, D. B. *Macromolecules* **2007**, *40* (16), 5959–5965.
(24) Gotze, I. O.; Archer, A. J.; Likos, C. N. *J. Chem. Phys.* 2006, *124* (8), art. no. 084901.
(25) Shi, X.; Bányai, I.; Rodriguez, K.; Islam, M. T.; Lesniak, W.; Balogh, P.; Balogh, L. P.; Baker, J. R. *Electrophoresis* **2006**, *27* (9), 1758–1767.
(26) Dillon, R. E. A.; Shriver, D. F. *Chem. Mater.* **2001**, *13* (4), 1369–1373.
(27) Wang, Z.; Ikeda, M.; Hirata, N.; Kubo, M.; Itoh, T.; Yamamoto, O. *J. Electrochem. Soc.* **1999**, *146* (6), 2209–2215.
(28) Hawker, C. J.; Chu, F.; Pomery, P. J.; Hill, D. J. T. *Macromolecules* **1996**, *29* (11), 3831–3838.
(29) Karatasos, K. *Macromolecules* **2008**, *41* (3), 1025–1033.
(30) Karatasos, K.; Krystallis, M. *Macromol. Symp.* **2009**, *278* (1), 32–39.
(31) Terao, T. *Chem. Phys. Lett.* **2007**, *446* (4−6), 350–353.
(32) Nisato, G.; Ivkov, R.; Amis, E. J. *Macromolecules* **1999**, *32* (18), 5895–5900.
(33) Maskaly, G. R.; Garcia, R. E.; Carter, W. C.; Chiang, Y. M. *Phys. Rev. E* 2006, *73* (1).
(34) Leunissen, M. E.; Christova, C. G.; Hynninen, A.-P.; Royall, C. P.; Campbell, A. I.; Imhov, A.; Dijkstra, M.; van Roij, R.; van Blaaderen, A. *Nature* **2005**, *437* (7056), 235.
(35) Karatasos, K.; Krystallis, M. *J. Chem. Phys.* **2009**, *130*, 114903.
(36) Bonincontro, A.; Cametti, C.; Nardiello, B.; Marchetti, S.; Onori, G. *Biophys. Chem.* **2006**, *121* (1), 7–13.
(37) Yethiraj, A.; van Blaaderen, A. *Nature* **2003**, *421*, 6922.
(38) Chai, M. H.; Niu, Y. H.; Youngs, W. J.; Rinaldi, P. L. *J. Am. Chem. Soc.* **2001**, *123* (20), 4670–4678.
(39) Niu, Y. H.; Crooks, R. A. *Chem. Mater.* **2003**, *15*, 3463.
(40) Liu, M.; Fréchet, J. M. J. *Polym. Bull.* **1999**, *43* (4), 379–386.
(41) Nisato, G.; Ivkov, R.; Amis, E. J. *Macromolecules* **2000**, *33* (11), 4172–4176.
(42) Gurtovenko, A. A.; Lyulin, S. V.; Karttunen, M.; Vattulainen, I. *J. Chem. Phys.* **2006**, *124* (9), 094904.
(43) Tian, W.-d.; Ma, Y.-q. *J. Phys. Chem. B* **2009**, *113* (40), 13161–13170.
(44) Huissmann, S.; Wynveen, A.; Likos, C. N.; Blaak, R. *J. Phys.: Condens. Matter* **2010**, *22* (23), 232101.
(45) Majtyka, M.; Klos, J. *Phys. Chem. Chem. Phys.* **2007**, *9* (18), 2284–2292.
(46) Guldbrand, L.; Nordenskiold, L. *J. Phys. Chem.* **1987**, *91* (22), 5714–5718.
(47) Quesada-Perez, M.; Callejas-Fernandez, J.; Hidalgo-Alvarez, R. *Adv. Colloid Interface Sci.* **2002**, *95* (2−3), 295–315.
(48) Martin-Molina, A.; Maroto-Centeno, J. A.; Hidalgo-Alvarez, R.; Quesada-Perez, M. *Colloids Surf., A* **2008**, *319* (1−3), 103–108.
(49) Furukawa, T.; Ishizu, K. *Macromolecules* **2003**, *36* (2), 434–439.
(50) Ohshima, A.; Konishi, T.; Yamanaka, J.; Ise, N. *Phys. Rev. E* **2001**, *64* (5), 051808.
(51) Tian, W.-d.; Ma, Y.-q. *Soft Matter* **2011**, *7* (2), 500–505.
(52) Angelini, T. E.; Liang, H.; Wriggers, W.; Wong, G. C. L. *Proc. Natl. Acad. Sci. U.S.A.* **2003**, *100* (15), 8634–8637.
(53) Angelini, T. E.; Golestanian, R.; Coridan, R. H.; Butler, J. C.; Beraud, A.; Krisch, M.; Sinn, H.; Schweizer, K. S.; Wong, G. C. L. *Proc. Natl. Acad. Sci. U.S.A.* **2006**, *103* (21), 7962–7967.
(54) Muthukumar, M. *J. Chem. Phys.* **2004**, *120* (19), 9343–9350.
(55) Karatasos, K. *Macromolecules* **2006**, *39*, 4619.
(56) Liu, J.; Palberg, T. Crystal growth and crystal morphology of charged colloidal binary mixtures. In *Trends in Colloid and Interface Science XVI*: Springer: Berlin and Heidelberg, Germany, 2004; Vol. 123, pp 222−226.
(57) Stradner, A.; Sedgwick, H.; Cardinaux, F.; Poon, W. C. K.; Egelhaaf, S. U.; Schurtenberger, P. *Nature* **2004**, *432* (7016), 492.
(58) Zallen, R., *The Physics of Amorphous Solids*. John Wiley and Sons Ltd.: New York, 1983.
(59) Wahnström, G. *Phys. Rev. A* **1991**, *44*, 3752.
(60) Karatasos, K.; Lyulin, A. V. *J. Chem. Phys.* **2006**, *125* (18), 184907.
(61) Lindemann, F. *Z. Phys.* **1910**, *11*, 609.
(62) Puertas, A. M.; Fuchs, A. Glasses in Colloidal Systems: Attractive Interactions and Gelation. In *Structure and Functional Properties of Collodal Systems*; Hidalgo-Álvarez, R., Ed. CRC Press: Boca Raton, FL, 2010; pp 135−164.
(63) Karatasos, K.; Adolf, D. B.; Davies, G. R. *J. Chem. Phys.* **2001**, *115* (11), 5310–5318.
(64) Markelov, D. A.; Lyulin, S. V.; Gotlib, Y. Y.; Lyulin, A. V.; Matveev, V. V.; Lahderanta, E.; Darinskii, A. A. *J. Chem. Phys.* **2009**, *130* (4), 044907–9.
(65) Moreno, K. X.; Simanek, E. E. *Macromolecules* **2008**, *41* (12), 4108–4114.
(66) Mijovic, J.; Ristic, S.; Kenny, J. *Macromolecules* **2007**, *40* (14), 5212–5221.
(67) Puertas, A. M.; Fuchs, M.; Cates, M. E. *Phys. Rev. Lett.* **2002**, *88* (9), 098301.
(68) Zaccarelli, E.; Mayer, C.; Asteriadi, A.; Likos, C. N.; Sciortino, F.; Roovers, J.; Iatrou, H.; Hadjichristidis, N.; Tartaglia, P.; Löwen, H.; Vlassopoulos, D. *Phys. Rev. Lett.* **2005**, *95* (26), 268301.